

Creation and manipulation of stable dark solitons and vortices in microcavity polariton condensates

Xuekai Ma¹, Oleg A. Egorov², and Stefan Schumacher¹

¹*Department of Physics and Center for Optoelectronics and Photonics Paderborn (CeOPP),
Universität Paderborn, Warburger Strasse 100, 33098 Paderborn, Germany and*

²*Institute of Condensed Matter Theory and Solid State Optics, Abbe Center of Photonics,
Friedrich-Schiller-Universität Jena, Max-Wien-Platz 1, 07743 Jena, Germany*

Solitons and vortices offer potential for use in information storage, processing, and communication. In semiconductor microcavities, stable propagating polariton solitons can be coherently excited. In incoherent excitation schemes, different types of solitons have been reported in polariton condensates. However, these have in common that soliton creation is random and solitons cannot be controlled after their creation. In the present work we demonstrate the existence of stable dark solitons and vortices under non-resonant incoherent excitation of a polariton condensate with a spatially periodic pump. In one dimension, we show that an additional coherent light pulse can be used to create or destroy a dark soliton in a controlled manner. In two dimensions we demonstrate that a coherent light beam can be used to move a vortex to a specific position on the lattice or be set into motion by simply switching the periodic pump structure from two-dimensional (lattice) to one-dimensional (stripes). Our theoretical results open up exciting possibilities to optically control dark solitons and vortices in polariton condensates.

Over the past decade, exciton-polaritons in quantum-well semiconductor microcavities with normal-mode splitting have attracted a lot of attention due to their exceptional properties. Exciton-polaritons are quasi particles formed from a cavity light field and a quantum well (QW) exciton [1]. These quasi particles possess both photonic and excitonic nature. They have a small effective mass ($\sim 10^{-4}m_e$, m_e is the free electron mass) and short lifetime on a picosecond time scale both inherited from the photonic part. Through their excitonic part they interact with each other and as composite Bosons they can undergo a non-equilibrium phase transition with similarities to Bose-Einstein condensation (BEC) [2–4], potentially even up to room temperature [5–7]. The interaction between polaritons leads to an effective optical nonlinearity that has led to the observation of a whole wealth of nonlinear phenomena some of which may find applications in quantum simulators or logical polariton devices, including bistability [8–10], pattern formation [11–14], vortices [15–17], and solitons [18–22].

Solitons and vortices are spatially localized stationary solutions of a nonlinear system. Generally speaking, only a focusing nonlinearity can support bright solitons, while dark solitons (which are low-density defects in the homogeneous phase) can only exist in a defocusing nonlinear system. Under resonant coherent excitation and using the non-parabolicity of the lower polariton branch, for polaritons in the same polarization state such that the nonlinearity is defocussing, however, the existence of both bright [18, 19] and dark [20–22] solitons propagating with a finite momentum was reported. Under non-resonant (incoherent) excitation, 2D phase defects (vortices) of polariton condensates are found to be stable in both the scalar and spin-dependent (spinor) cases [14]. However, during the condensation process these entities

are randomly created and they cannot be controlled. For the spinor system in 1D, the existence of stable dark soliton trains has been reported [23]. In the scalar system, dark solitons are unstable and can only persist for some time but then disappear as the system transitions into the stable homogeneous phase in 1D [24]. In 2D unstable dark solitons split up into several vortex-antivortex pairs [25].

In the present work, we study the dynamics of polariton condensates under non-resonant excitation with a periodic pump profile. We demonstrate the existence, controlled creation, annihilation, and manipulation of stable dark solitons. During the condensation, dark solitons form spontaneously and are confined inside the valleys of the periodic pump profile. When using a spatially homogenous pump first and introducing periodicity in a second step, a fully periodic condensate solution (without any dark solitons) can also be excited. We demonstrate that in this fully periodic solution, dark solitons can then be created and annihilated at desired spatial positions with short coherent light pulses at $k = 0$ (normal incidence).

We also find stable phase defects for periodic excitation in 2D, so-called vortices. For periodic excitation, we find two kinds of vortices: smaller-sized vortices are trapped inside one of the pump valleys and larger-sized vortices have their centers at one the pump profile maxima (in a valley of the periodic condensate solution). Both types of vortices are pinned to their initial position on the 2D lattice. However, we demonstrate that a coherent light beam at $k = 0$ can help a vortex escape its potential trap such that it is free to move to an adjacent cell, following the motion of the coherent beam on the 2D lattice. Additionally, the vortices can also be controlled switching the non-resonant periodic pump from a 2D lattice to stripes

in 2D, setting already existing vortices into motion along the stripes.

Model – To study the dynamics in a polariton condensate we use a standard mean-field theory and assume the formation of an exciton-polariton condensate at the bottom of the lower-polariton branch. A driven-dissipative Gross-Pitaevskii (GP) model can be used to describe the condensate dynamics coupled to an exciton reservoir excited by a non-resonant pump source [26].

$$i\hbar \frac{\partial \Psi(\mathbf{r}, t)}{\partial t} = \left[-\frac{\hbar^2}{2m} \nabla_{\perp}^2 - i\hbar \frac{\gamma_c}{2} + g_c |\Psi(\mathbf{r}, t)|^2 + \left(g_r + i\hbar \frac{R}{2} \right) n(\mathbf{r}, t) \right] \Psi(\mathbf{r}, t) + P_c(\mathbf{r}, t), \quad (1)$$

$$\frac{\partial n(\mathbf{r}, t)}{\partial t} = [-\gamma_r - R|\Psi(\mathbf{r}, t)|^2] n(\mathbf{r}, t) + P_i(\mathbf{r}, t). \quad (2)$$

Here $\Psi(\mathbf{r}, t)$ is the coherent polariton field and $n(\mathbf{r}, t)$ is the exciton reservoir density. $m = 10^{-4}m_e/a$ is the effective mass of polaritons on the lower branch (m_e is the free electron mass), with a parameter a which can be adjusted to consider different detunings of the cavity mode from the quantum well exciton resonance. Due to the finite life time of cavity photons, polaritons decay with γ_c . The polariton condensate is replenished by the coupling to the reservoir density $n(\mathbf{r}, t)$ with $R = 0.01 \text{ ps}^{-1} \mu\text{m}^2$. In addition, a coherent pulse, $P_c(\mathbf{r}, t)$, can be used to excite the condensate. $g_c = 6 \times 10^{-3} \text{ meV} \mu\text{m}^2$ represents the nonlinear interaction between polaritons, and $g_r = 2g_c$ is the interaction between polaritons and reservoir excitons [17]. Reservoir excitons are generated through the source term $P_i(\mathbf{r}, t)$ with periodic spatial distribution as shown in Fig. 1(a). The one- and two-dimensional periodic pump structures are generated by interfering two (or four, respectively) coherent plane waves as illustrated. The reservoir density is assumed to decay with $\gamma_r = 1.5\gamma_c$ [17].

1D excitation – First we study a one-dimensional system where polaritons are confined in a wire in the cavity plane. Such a structure can be realized using a number of different techniques [27–35]. The periodic pump source is given by $P_i(x) = P \sin^2(\pi x/d)$ with the period $d = 8 \mu\text{m}$ as illustrated in Fig. 1(a). For a continuous wave source, Fig. 1(b) shows the region of existence of periodic stationary solutions depending on the pump intensity P . When the pump intensity is above condensation threshold and not too high with $2 \lesssim P \lesssim 12$, the density distribution of the periodic condensate solution is similar to the periodic reservoir density $n(x)$ and pump distribution. That is, the minimum density of the condensate solution resides in the valleys of the pump density at $x = dN$, $N = 0, \pm 1, \pm 2, \dots$ as shown in the inset of Fig. 1(b). However, when the pump intensity is larger with $P > 14$, the periodic reservoir density acts as a periodic potential trapping condensate density inside

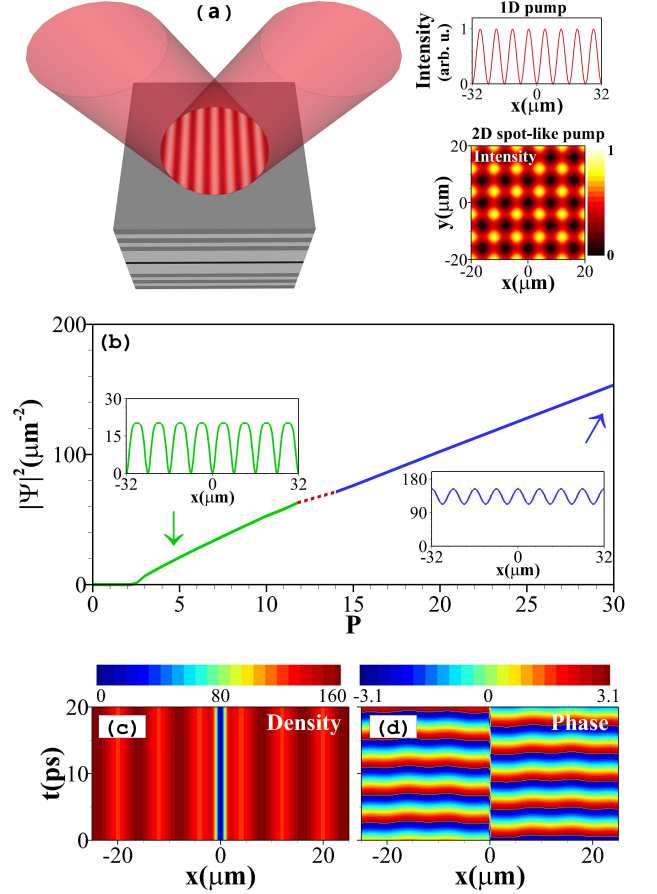


FIG. 1. (Color online) (a) Sketch of a semiconductor microcavity with a quantum well (QW) sandwiched between two distributed Bragg reflectors (DBRs). Two coherent homogeneous optical beams create a periodically oscillating excitation reservoir. The two panels on the right illustrate the periodic pump profiles in 1D and 2D. The 2D periodic structure is generated by four coherent homogeneous beams. (b) Density distribution (in μm^{-2}) of steady state periodic solutions of the polariton condensate created by periodic pumps in 1D. Solid lines represent stable solutions, while the dashed line represents unstable solutions. The insets show the solutions at $P = 5$ and $P = 30$, respectively. Time evolution of (c) the density and (d) the phase of a stable dark soliton in 1D at $P = 30$.

the valleys such that the maximum condensate density is found in the valleys of the pump at $x = dN + d/2$. The transition between these different types of solutions occurs in the small region of $12 \lesssim P \lesssim 14$, where no stable stationary solutions are found numerically. Interestingly, we find that in the region with $P > 14$, besides the periodic solutions discussed above, also stable stationary solutions exist where a dark soliton forms in one or multiple of the pump valleys. Figure 1(c) shows an example with a dark soliton at $x = 0$. The drop in density at $x = 0$ is accompanied by a π shift in phase as shown in Fig. 1(d).

In the real system, the onset of condensate formation

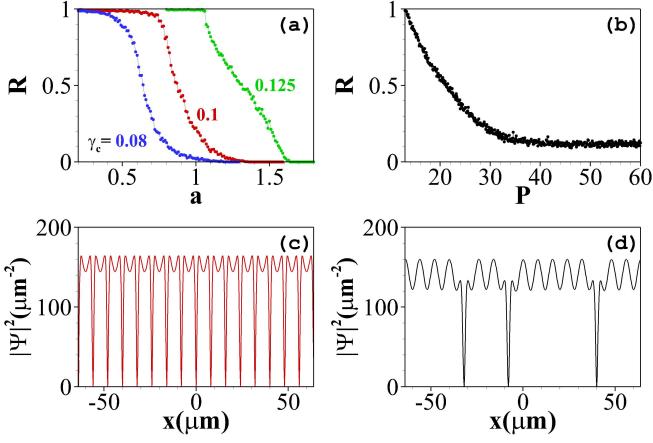


FIG. 2. (Color online) Density of dark solitons for different system parameters. (a) Dependence of the number of dark solitons per number of pump valleys, R , on the effective polariton mass (scaled with the factor a) at $P = 30$ for $\gamma_c = 0.08 \text{ ps}^{-1}$, $\gamma_c = 0.1 \text{ ps}^{-1}$, and $\gamma_c = 0.125 \text{ ps}^{-1}$. (b) Dependence of R on the pump intensity with $a = 1$ and $\gamma_c = 0.1 \text{ ps}^{-1}$. Profiles of dark solitons with (c) $\gamma_c = 0.1 \text{ ps}^{-1}$, $a = 0.5$, and $P = 30$, and with (d) $\gamma_c = 0.1 \text{ ps}^{-1}$, $a = 1$, and $P = 30$.

occurs spontaneously. To mimic this process in the numerical calculations, initial condensate formation is triggered by a spatially randomly varying initial condition for $\Psi(\mathbf{r}, t)$, which is different in each run of a calculation. Depending on the exact initial condition, the system assumes different stationary solutions as it evolves in time. These may contain different numbers of dark solitons, depending on the initial presence of phase defects near pump valleys but equally importantly depending on system parameters such as dissipation and effective mass [14]. These parameters determine polariton lifetime and mobility and with that crucially influence the robustness of initial phase defects as the condensate reached a quasi-equilibrium state. In order to quantify the number of dark solitons formed during the condensation process depending on system parameters, we define the ratio $R = \frac{\text{number of dark solitons}}{\text{number of pump valleys}}$, with $0 \leq R \leq 1$. Figure 2(a) illustrates how the number of dark solitons formed depends on polariton loss γ_c effective mass parameter a for random noisy initial conditions and fixed pump intensity. For fixed γ_c the number of dark solitons formed increases with increasing effective mass (decreasing parameter a). When the polariton mobility is reduced at smaller a , more phase defects in the initial noise survive. At $R = 1$, dark solitons are formed at each pump valley as shown in Fig. 2(c). Fig. 2(d) shows a case for larger effective mass where only few dark solitons are formed (in positions determined by the initial noise). For $R \rightarrow 0$ no dark solitons survive. For fixed a , $a = 1$ for instance, the spatial correlations inside the condensate are more pronounced if the polaritons have

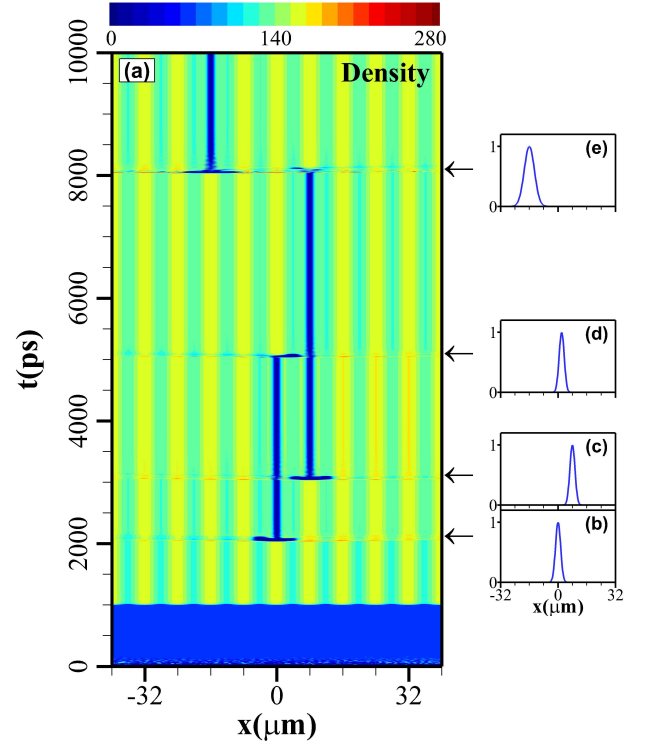


FIG. 3. (Color online) Controlled excitation and switching dynamics of dark solitons. (a) Time evolution of the condensate density (in μm^{-2}) under homogeneous ($t < 1000 \text{ ps}$) and periodic ($t \geq 1000 \text{ ps}$) excitation at $P = 30$. (b)-(e) Normalized spatial intensity profiles of coherent pulse used for creation and annihilation of dark solitons launched at different times and spatial positions (b) $x = 0 \mu\text{m}$, (c) $x = 8 \mu\text{m}$, (d) $x = 2 \mu\text{m}$, (e) $x = -16 \mu\text{m}$.

a longer lifetime (smaller γ_c), resulting in the formation of less dark solitons. In summary, the less mobile the polaritons and the shorter their lifetime the larger the number of dark solitons formed from initial noise. The number of dark solitons formed further depends on the pump intensity [14] as shown in Fig. 2(b) for fixed γ_c and a .

In experiments on microcavity polaritons, initial conditions are always noisy. Therefore it will be difficult to excite the pure periodic solutions, a single dark soliton, or a dark soliton at a specified pump valley. However, creating a single dark soliton in a controlled manner is very important first step in gaining control over solitons. In Fig. 3 we present an approach where we use the fact that dark solitons are unstable under homogeneous excitation [24] such that a homogeneously pumped system eventually assumes a homogeneous solution also for the condensate. We use the excitation scenario illustrated in Fig. 1(a) with a time delay (here one nanosecond) between the two pump beams. The beam arriving first excites a homogeneous condensate solution [$t < 1000 \text{ ps}$ in

Fig. 3(a)]. Then, the second beam arrives and interferes with the first beam periodically modulating the pump profile. This periodic modulation is also transferred to the condensate for which a periodic solution forms without generation of any dark solitons [$1000 \text{ ps} \leq t < 2000 \text{ ps}$ in Fig. 3(a)]. After initialization of this periodic condensate state, an additional resonant (coherent) pulse with $3 \mu\text{m}$ width and 80 ps duration [Fig. 3(b)] is used to create a dark soliton in the valley at $x = 0$. Previously it was reported that such a coherent pulse with Gaussian shape suffers a depletion at its center and the condensate forms a ring shape because of propagation of the condensate away from the source [36]. In Fig. 3(a) a region with low polariton density is generated near $x = 0 \mu\text{m}$ after the injection of the coherent pulse at $t = 2000 \text{ ps}$. At the same time the phase coherence is disturbed and a dark soliton is created. With another coherent pulse at $t = 3000 \text{ ps}$ we create another dark soliton in a neighboring pump valley. With the same approach further dark solitons can be created until all the pump valleys are occupied. As the dark solitons only survive in the pump valleys, the same coherent pulses centered at a pump maximum next to the two existing dark soliton (for example at $x = 4 \mu\text{m}$) could be used to simultaneously annihilate both neighboring dark solitons at $x = 0 \mu\text{m}$ and $x = 8 \mu\text{m}$ (this scenario is not shown in Fig. 3). If the coherent pulse is launched closer to one of the two solitons [at $x = 2 \mu\text{m}$ in Fig. 3(d)], the nearest dark soliton at $x = 0 \mu\text{m}$ is annihilated whereas the other (at $x = 8 \mu\text{m}$) survives as shown in Fig. 3(a) ($5000 \text{ ps} < t < 8000 \text{ ps}$). While, a broader coherent pulse with width of $6 \mu\text{m}$ [Fig. 3(e)] and 50 ps duration can be used to annihilate a dark soliton in a more distant pump valley and simultaneously create a new dark soliton where the broader pulse is injected. We would like to emphasize that the control demonstrated is very robust and in particular not sensitive to the phase of the applied light pulses, nor does it require precise tuning of the pulse frequency.

2D excitation – Previously it was reported that in a two-dimensional system a homogeneous pump supports stable vortices in polariton condensates both in the scalar and spinor cases [14], where initial phase defects survive the condensate formation according to the Kibble-Zurek theory. In the present work we use excitation with a 2D periodic lattice given by $P_i(x, y) = P(\sin^2(\pi x/8) + \sin^2(\pi y/8))$ as illustrated in Fig. 1(a). For this type of excitation configuration, we find two different types of vortices that form from the initial noise as illustrated in Figs. 4(a) and (b). One type resides in the pump valleys (the maxima of the condensate background) and has a smaller size. The other type has a larger size and forms in the pump maxima (the valleys of the condensate background). As shown in Fig. 4(d) the total number of vortices initially increases with increasing pump intensity [$P < 14$], analogously to the scaling laws discussed in [14]. For larger pump intensity [$P > 14$], however, due

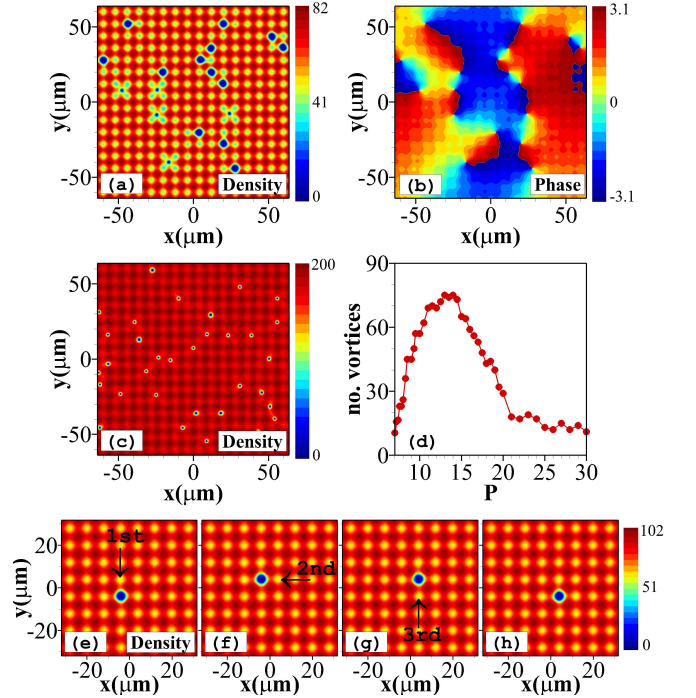


FIG. 4. (Color online) Controlling vortices with coherent pulses. Profiles of (a) density (in μm^{-2}) and (b) phase of condensate under 2D periodic pump excitation at $P = 8$ showing vortices (phase defects) forming from the initial noise. (c) Density profile of condensate at $P = 20$. (d) Dependence of number of vortices on pump intensity. (e)-(h) Manipulation of a vortex by a sequence of four coherent pulses at $P = 10$. Snapshots of the density profiles (in μm^{-2}) are shown at (e) $t = 400 \text{ ps}$, (f) $t = 800 \text{ ps}$, (g) $t = 1200 \text{ ps}$, and (h) $t = 1400 \text{ ps}$. A full movie is included in the Supplemental Material. Arrows indicate the target cell for vortex motion due to application of a coherent pulse.

to saturation effects the periodic condensate background is more similar to the homogeneous solution reducing the total number of vortices. Moreover, the size of vortices becomes smaller for larger pump intensity as shown in Fig. 4(c). For increasing pump intensity vortices more easily move out of their cells and interact with adjacent vortices. A vortex and an anti-vortex attract each other and both are annihilated when they are too close. This explains the decrease in the number of vortices for pump intensity $P > 14$. To generate Fig. 4(d), the number of vortices is counted when the polariton and reservoir densities reach a steady state.

Unlike the controlled creation of dark solitons by coherent pulses in the 1D case discussed above, it has proven more difficult to create a vortex (2D phase defect) in the 2D periodic condensate. We find, however, that coherent pulses can be used to re-locate an existing vortex from its original cell on the lattice to a neighboring cell as shown in Fig. 4 (a movie showing the dynamics of manipulation is available in the Supplemental Material).

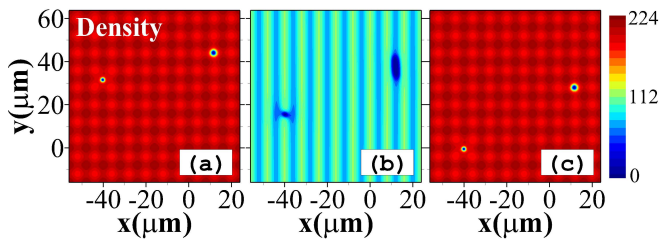


FIG. 5. (Color online) Controlling vortices through non-resonant excitation. Shown is the manipulation of vortices by switching the excitation from a two-dimensional lattice (with two vortices) in (a) to a stripe-like excitation in (b), setting the vortices into motion, back to a two-dimensional lattice confining the vortices in a different place in (c). The panels show snapshots of the condensate density (in μm^{-2}) in time for $P = 22$ at (a) $t = 400$ ps, (b) $t = 800$ ps, and (c) $t = 1200$ ps. A corresponding movie is included in the Supplemental Material.

In Figs. 4(e)-(h) we use a sequence of four pulses, each $3\mu\text{m}$ in diameter and 80 ps in length. We find that a coherent pulse creates a reduced condensate density at its center. Applied next to an existing vortex this can be used to reduce the effective potential confining the vortex on one side. Through this pulse-induced opening in the potential barrier the vortex is then released. Applying a series of pulses in different spatial positions, a vortex can be systematically moved around on the two-dimensional lattice, in principle enabling the generation of any desired regular or irregular arrangement of vortices.

Finally we would like to discuss that the motion of vortices in 2D can also be manipulated without the need for excitation with coherent pulses, only modifying the source that generates the periodic reservoir density. Here we make use of the fact that in 2D for a periodic pump profile along one direction (stripe-like, with $P_i(x, y) = P \sin^2(\pi x/8)$), also two kinds of vortices exist. However, in the configuration with stripes in y -direction the vortices can move freely along this direction. This can be used to control the position of vortices after creation on a 2D lattice. For example, consider a case where two vortices were created by a 2D periodic pump lattice as in Fig. 5(a). If subsequently switching to a stripe-like pump profile as in Fig. 5(b), the two vortices move along the y axis. When switching back to the 2D lattice at a later point in time as in Fig. 5(c) the two vortices are trapped in a different place on the lattice. A movie showing the full time evolution is included in the Supplemental Material. Analogously, the vortices can be moved along the x -direction. However, we note that the direction of motion (forward or backward) and the velocity acquired by the vortices is not easy to predict in this simple scheme, as it is influenced by the phase distribution and the interactions between vortices.

Conclusion – To summarise, we found that when creat-

ing a polariton condensate with a spatially periodic pump source, phase defects are stabilized in both 1D (as dark solitons) and 2D (as vortices). In 1D we demonstrate that dark solitons are either generated randomly from the initial noise triggering condensation or – more importantly – can be created on demand by a coherent light pulse. In 2D, we find two kinds of stable vortices which can also be optically manipulated and flexibly moved on a 2D lattice by use of coherent light pulses. We further demonstrate that vortices in 2D can also be manipulated using only non-resonant (incoherent) optical means. Our findings open up exciting possibilities to use solitons and vortices in polariton condensates for information storage and processing or quantum simulators.

This work was supported by the Deutsche Forschungsgemeinschaft (DFG) through the collaborative research center TRR 142. S.S. acknowledges support through the Heisenberg programme of the DFG.

-
- [1] C. Weisbuch, M. Nishioka, A. Ishikawa, and Y. Arakawa, *Phys. Rev. Lett.* **69**, 3314, 1992.
 - [2] H. Deng, G. Weihs, C. Santori, J. Bloch, and Y. Yamamoto, *Science* **298**, 199 (2002).
 - [3] J. Kasprzak, M. Richard, S. Kundermann, A. Baas, P. Jeambrun, J. M. J. Keeling, F. M. Marchetti, M. H. Szymańska, R. André, J. L. Staehli, V. Savona, P. B. Littlewood, B. Deveaud, and Le Si Dang, *Nature* **443**, 409 (2006).
 - [4] H. Deng, H. Haug, and Y. Yamamoto, *Rev. Mod. Phys.* **82**, 1489 (2010).
 - [5] S. Christopoulos, G. Baldassarri, Höger von Högersthal, A. J. D. Grundy, P. G. Lagoudakis, A.V. Kavokin, J. J. Baumberg, G. Christmann, R. Butté, E. Feltin, J.-F. Carlin, and N. Grandjean, *Phys. Rev. Lett.* **98**, 126405 (2007).
 - [6] G. Christmann, R. Butté, E. Feltin, J.-F. Carlin, and N. Grandjean, *Appl. Phys. Lett.* **93**, 051102 (2008).
 - [7] J. J. Baumberg, A. V. Kavokin, S. Christopoulos, A. J. D. Grundy, R. Butté, G. Christmann, D. D. Solnyshkov, G. Malpuech, G. Baldassarri Höger von Högersthal, E. Feltin, J.-F. Carlin, and N. Grandjean, *Phys. Rev. Lett.* **101**, 136409 (2008).
 - [8] A. Tredicucci, Y. Chen, V. Pellegrini, M. Börger, and F. Bassani, *Phys. Rev. A* **54**, 3493 (1996).
 - [9] A. Baas, J. P. Karr, H. Eleuch, and E. Giacobino, *Phys. Rev. A* **69**, 023809 (2004).
 - [10] D. Bajoni, E. Semenova, A. Lemaitre, S. Bouchoule, E. Wertz, P. Senellart, S. Barbay, R. Kuszelewicz, and J. Bloch, *Phys. Rev. Lett.* **101**, 266402 (2008).
 - [11] M. O. Borgh, J. Keeling, and N. G. Berloff, *Phys. Rev. B* **81**, 235302 (2010).
 - [12] M. H. Luk, Y. C. Tse, N. H. Kwong, P. T. Leung, P. Lewandowski, R. Binder, and Stefan Schumacher, *Phys. Rev. B* **87**, 205307 (2013).
 - [13] A. Werner, O. A. Egorov, and F. Lederer, *Phys. Rev. B* **89**, 245307 (2014).
 - [14] T. C. H. Liew, O. A. Egorov, M. Matuszewski, O. Kyriienko, X. Ma, and E. A. Ostrovskaya, *Phys. Rev. B* **91**,

- 085413 (2015).
- [15] K. G. Lagoudakis, M. Wouters, M. Richard, A. Baas, I. Carusotto, R. André, Le Si Dang, and B. Deveaud-Plédran, *Nat. Phys.* **4**, 706 (2008).
 - [16] K. G. Lagoudakis, T. Ostatnický, A. V. Kavokin, Y. G. Rubo, R. André, B. Deveaud-Plédran, *Science* **326**, 974 (2009).
 - [17] G. Roumpos, M. D. Fraser, A. Löffler, S. Höfling, A. Forchel, and Y. Yamamoto, *Nat. Phys.* **7**, 129 (2011).
 - [18] O. A. Egorov, D. V. Skryabin, A. V. Yulin, and F. Lederer, *Phys. Rev. Lett.* **102**, 153904 (2009).
 - [19] M. Sich, D. N. Krizhanovskii, M. S. Skolnick, A. V. Gorbach, R. Hartley, D. V. Skryabin, E. A. Cerda-Méndez, K. Biermann, R. Hey, and P. V. Santos, *Nat. Photonics* **6**, 50 (2012).
 - [20] A. V. Yulin, O. A. Egorov, F. Lederer, and D. V. Skryabin, *Phys. Rev. A* **78**, 061801(R) (2008).
 - [21] G. Grosso, G. Nardin, F. Morier-Genoud, Y. Léger, and B. Deveaud-Plédran, *Phys. Rev. B* **86**, 020509(R) (2012).
 - [22] P. Cilibrizzi, H. Ohadi, T. Ostatnický, A. Askitopoulos, W. Langbein, and P. Lagoudakis, *Phys. Rev. Lett.* **113**, 103901 (2014).
 - [23] F. Pinsker and H. Flayac, *Phys. Rev. Lett.* **112**, 140405 (2014).
 - [24] Y. Xue and M. Matuszewski, *Phys. Rev. Lett.* **112**, 216401 (2014).
 - [25] L. A. Smirnov, D. A. Smirnova, E. A. Ostrovskaya, and Y. S. Kivshar, *Phys. Rev. B* **89**, 235310 (2014).
 - [26] M. Wouters and I. Carusotto, *Phys. Rev. Lett.* **99**, 140402 (2007).
 - [27] E. Wertz, L. Ferrier, D. D. Solnyshkov, R. Johné, D. Sanvitto, A. Lemaître, I. Sagnes, R. Grousson, A. V. Kavokin, P. Senellart, G. Malpuech, and J. Bloch, *Nature Phys.* **6**, 860 (2010).
 - [28] R. I. Kaitouni, O. El Daïf, A. Baas, M. Richard, T. Paraiso, P. Lugan, T. Guillet, F. Morier-Genoud, J. D. Ganière, J. L. Staehli, V. Savona, and B. Deveaud, *Phys. Rev. B* **74**, 155311 (2013).
 - [29] E. A. Cerda-Méndez, D. N. Krizhanovskii, M. Wouters, R. Bradley, K. Biermann, K. Guda, R. Hey, P. V. Santos, D. Sarkar, and M. S. Skolnick, *Phys. Rev. Lett.* **105**, 116402 (2010).
 - [30] C. W. Lai, N. Y. Kim, S. Utsunomiya, G. Roumpos, H. Deng, M. D. Fraser, T. Byrnes, P. Recher, N. Kumada, T. Fujisawa, and Y. Yamamoto, *Nature (London)* **450**, 529 (2007).
 - [31] N. Y. Kim, K. Kusudo, C. Wu, N. Masumoto, A. Löffler, S. Höfling, N. Kumada, L. Worschech, A. Forchel, and Y. Yamamoto, *Nat. Phys.* **7**, 681 (2011).
 - [32] D. Tanese, H. Flayac, D. Solnyshkov, A. Amo, A. Lemaître, E. Galopin, R. Braive, P. Senellart, I. Sagnes, G. Malpuech, and J. Bloch, *Nature Comm.*, **4**, 1749 (2013).
 - [33] F. Baboux, L. Ge, T. Jacqmin, M. Biondi, E. Galopin, A. Lemaître, L. Le Gratiet, I. Sagnes, S. Schmidt, H. E. Türeci, A. Amo, and J. Bloch, *Phys. Rev. Lett.* **116**, 066402 (2016).
 - [34] K. Winkler, J. Fischer, A. Schade, M. Amthor, R. Dall, J. Geßler, M. Emmerling, E. A. Ostrovskaya, M. Kamp, C. Schneider, and S. Höfling, *New J. Phys.* **17**, 023001 (2015).
 - [35] K. Winkler, O. A. Egorov, I. G. Savenko, X. Ma, E. Estrecho, T. Gao, S. Müller, M. Kamp, T. C. H. Liew, E. A. Ostrovskaya, S. Höfling, and C. Schneider, *Phys. Rev. B* **93**, 121303(R) (2016).
 - [36] L. Dominici, M. Petrov, M. Matuszewski, D. Ballarini, M. De Giorgi, D. Colas, E. Cancellieri, B. Silva Fernández, A. Bramati, G. Gigli, A. Kavokin, F. Laussy, and D. Sanvitto, *Nat. Commun.* **6**, 8993 (2015).